Editors' Suggestion

Generalized dispersion Kerr solitons

Kevin K. K. Tam* and Tristram J. Alexander
Institute of Photonics and Optical Science, School of Physics, University of Sydney, Sydney, New South Wales 2006, Australia

Andrea Blanco-Redondo
Nokia Bell Labs, 791 Holmdel Road, Holmdel, New Jersey 07733, USA

C. Martijn de Sterke†
Institute of Photonics and Optical Science, School of Physics, and University of Sydney Nano Institute, University of Sydney, Sydney, New South Wales 2006, Australia

(Received 20 October 2019; accepted 6 February 2020; published 17 April 2020)

We report a continuum of pulselike soliton solutions to the generalized nonlinear Schrödinger equation with both quadratic and quartic dispersion and a Kerr nonlinearity. We show that the well-known nonlinear Schrödinger solitons, which occur in the presence of only negative (anomalous) quadratic dispersion, and pure-quartic solitons, which occur in the presence of only negative quartic dispersion, are members of a large superfamily, encompassing both. The members of this family, none of which are unstable, have exponentially decaying tails, which can exhibit oscillations. We find analytic solutions for positive quadratic dispersion and negative quartic dispersion and investigate the soliton dynamics. We also find evidence that a combination of the quadratic and quartic dispersion, rather than exclusively quadratic or quartic dispersion, is likely to improve the performance of soliton lasers.

DOI: 10.1103/PhysRevA.101.043822

I. INTRODUCTION

Nonlinear Schrödinger (NLS) solitons, solitons that are solutions to the nonlinear Schrödinger equation, have been widely studied and have enabled a plethora of applications. They occur in a great variety of fields, including water waves [1], Bose-Einstein condensates [2,3], and plasmas [4]. In an optics context, they are characterized by quadratic dispersion and a Kerr nonlinear medium, i.e., a medium in which the refractive index depends linearly on intensity [5]. Many generalizations have been studied over the past decades, particularly higher-order nonlinearities [6], and more complicated geometries [7] with coupled modes involving different waveguides, polarizations, frequencies, propagation directions, or combinations of these. In comparison to this, deviations from perfectly quadratic dispersion have not been widely studied and have generally been treated as a perturbation of NLS solitons. Recently we studied Kerr nonlinear media at a frequency where the dispersion is purely quartic and demonstrated experimentally and theoretically that in such media pure quartic solitons (PQSs) can arise [8,9]. Though the experiments were carried out in a photonic crystal waveguide, PQSs should similarly occur in optical fibers [10] and in microresonators [11].

In practice it is difficult to achieve purely quadratic or purely quartic dispersion. We therefore consider here Kerr nonlinear media in the presence of both quadratic and quartic dispersion, without treating either as a perturbation. We take the quartic dispersion coefficient to be negative ($\beta_4 < 0$), whereas the quadratic dispersion coefficient (β_2) can have either sign. Nonlinear pulse propagation in the presence of negative β_2 and negative β_4 has been considered earlier [12–19]. Karlsson and Höök [12] found pulselike analytic solutions in the form of a squared hyperbolic secant, whereas Akhmediev *et al.* [13] found that, depending on the parameters, the exponentially decaying tails of these solutions can have additional oscillations. Akhmediev and Buryak [14] studied the interactions between the solitons and also showed [15] that the solutions with the oscillating tails may form bound states. The properties of these bound states depend on the relative alignment of the oscillations. Piché *et al.* [16] rederived the solutions found by Karlsson and Höök, and also considered the effect of nonzero β_3. More recently, Roy and Biancalana [17] considered the propagation of high-intensity pulses in specially designed slot waveguides in numerical experiments. By considering a geometry that minimizes Raman scattering, they found that it is possible to generate a large number of solitons, the spectral interference of which leads to a continuum. The work of Bansal *et al.* [18] and Biswas *et al.* [19] concentrates on finding analytic solutions in the presence of quartic and cubic dispersion.

In this paper, we demonstrate that NLS solitons and PQSs are in fact part of a single continuous soliton superfamily, which we refer to as generalized dispersion Kerr solitons (GDKSs), that also includes the set of analytic solutions for $\beta_2 < 0$ and $\beta_4 < 0$ reported by Karlsson and Höök [12]. By considering the tails of the solutions we can, based on analytic arguments, divide the parameter space into three distinct

*ktam6495@uni.sydney.edu.au
†martijn.desterke@sydney.edu.au

areas: (i) a region where the solutions have straight exponential tails, (ii) a region where the solutions have exponential tails with oscillations, and (iii) a region where no pulselike solutions exist. We find that near the boundary of regions (ii) and (iii) the solutions take the form of a carrier with a slowly varying envelope, and we show that the envelope, which in fact is the envelope of an envelope, satisfies the nonlinear Schrödinger equation.

All solitons (NLS solitons, PQSs, dissipative solitons, etc.) have applications in lasers, where they facilitate the formation of well-defined short pulses. However, soliton lasers, which currently exploit only quadratic dispersion, are limited to low energies. Though we do not perform a detailed laser analysis, we discuss the potential of GDKSs for use in ultrafast lasers and show that the presence of quartic dispersion may improve the laser performance. This potential application of PQSs was hinted at as early as 1994 [20], and only recently experimentally demonstrated by some of us [Runge *et al.*], but was never systematically investigated.

The outline of this paper is as follows: In Sec. II we review current knowledge of solitons with quadratic and quartic dispersion. In Sec. III we demonstrate that conventional NLS solitons and PQSs are members of a single superfamily. Then in Sec. IV we classify the members of this superfamily based on the behavior of their tails. In Sec. V we consider approximate analytic solutions in a limiting case. The scaling of the solutions is discussed in Sec. VI, followed in Sec. VII by a discussion of the effects of cubic dispersion, and a discussion in Sec. VIII of the dynamics of the solutions. Finally, in Sec. IX we discuss our results and conclude.

II. BACKGROUND

The propagation of high-intensity nonlinear pulses in optical fibers is described by the nonlinear Schrödinger equation [5]

$$i\frac{\partial\psi}{\partial z}-\frac{\beta_2}{2}\frac{\partial^2\psi}{\partial\tau^2}+\gamma|\psi|^2\psi=0, \tag{1}$$

where ψ is the complex envelope of the electric field which modulates the underlying carrier wave, τ is the retarded time in the frame of the pulse, z is the propagation distance, β_2 is the quadratic dispersion parameter obtained by Taylor expansion of the dispersion relation about the carrier frequency, and γ is the nonlinear parameter. The nonlinear Schrödinger equation (1) is integrable and has soliton solutions [5]. These maintain their hyperbolic secant shape upon propagation by balancing anomalous quadratic dispersion ($\beta_2<0$) with positive Kerr nonlinearity ($\gamma>0$) [21] and take the form

$$\psi(\tau,z)=\sqrt{\frac{2\mu}{\gamma}}\,\mathrm{sech}\left(\sqrt{\frac{2\mu}{|\beta_2|}}\tau\right)e^{i\mu z}, \tag{2}$$

where parameter μ gives the rate of change of the phase due to the nonlinearity. Different values of μ correspond to different particular solutions, taken from a family of conventional solitons with the same shape, but varying peak powers and widths. In this case, peak power increases monotonically with μ.

In 2016, Blanco-Redondo *et al.* experimentally discovered PQSs in a photonic crystal waveguide at a carrier frequency where β_2 and the cubic dispersion parameter β_3 were practically negligible [8]. Instead, the leading order of dispersion was quartic, so that the pulse envelope is described by a generalized NLS equation

$$i\frac{\partial\psi}{\partial z}+\frac{\beta_4}{24}\frac{\partial^4\psi}{\partial\tau^4}+\gamma|\psi|^2\psi=0, \tag{3}$$

where β_4 is the quartic dispersion parameter. While this equation is nonintegrable, in a recent comprehensive paper [9] we numerically demonstrated the existence and stability of PQSs for $\beta_4<0$, with temporal profiles characterized by exponentially decaying tails with additional oscillations. PQSs obey a favorable energy-width scaling $U\sim w^{-3}$, as opposed to $U\sim w^{-1}$ for NLS solitons [9]. Since Eq. (3) is nonintegrable, PQSs are technically not solitons. But for convenience, we use the term "soliton" for the solutions discussed in this paper.

Here we consider pulse propagation and the existence of solitons under the combined effects of different orders of dispersion. Higher orders of dispersion have traditionally been treated as perturbations to the NLS solitons, becoming important for subpicosecond pulses because of their large bandwidths. We consider the generalized nonlinear Schrödinger equation

$$i\frac{\partial\psi}{\partial z}-\frac{\beta_2}{2}\frac{\partial^2\psi}{\partial\tau^2}+\frac{\beta_4}{24}\frac{\partial^4\psi}{\partial\tau^4}+\gamma|\psi|^2\psi=0, \tag{4}$$

where β_2 and β_4 are obtained by Taylor expansion of the dispersion relation about the frequency ω_0 where $\beta_3=0$. Over the last decades, a number of authors have considered this equation [12,13,15–17], all of whom considered $\beta_2<0$ and $\beta_4<0$. In particular, in 1994 Karlsson and Höök [12] reported analytic solutions (for $\beta_2<0$ and $\beta_4<0$)

$$\psi(\tau,z)=3\sqrt{\frac{\beta_2^2}{5\beta_4}}\,\mathrm{sech}^2\left(\sqrt{\frac{3\beta_2}{\beta_4}}\tau\right)\exp\left(i\frac{24\beta_2^2}{25|\beta_4|}z\right), \tag{5}$$

with an equivalent solution later reported by Piché *et al.* [16]. Unlike the PQS, the temporal profile of Eq. (5) has exponentially decaying tails. For each value of β_2 and β_4, there exists a single solution (5) with fixed peak power, width, and

$$\mu=\frac{24\beta_2^2}{25|\beta_4|}. \tag{6}$$

This should be contrasted with NLS solitons and PQSs, where μ remains a free parameter. The isolated solution (5) can be understood by examining the scaling properties of Eq. (4). Among the four terms in Eq. (4), only three quantities (ψ,z,τ) can be rescaled for fixed values of β_2, β_4, and γ. As such, the scaling relations observed for NLS solitons and PQSs do not apply. However, we see in Sec. VI that in the presence of both β_2 and β_4 a more general scaling relation can be established.

NLS solitons are solutions for $\beta_2<0$ and $\beta_4=0$, and PQSs exist when $\beta_4<0$ and $\beta_2=0$, whereas the isolated solutions of Karlsson and Höök exist for $\beta_2<0$ and $\beta_4<0$. The natural question is whether these three types of solution are related to each other and whether other related types of solution are possible. We now turn to these questions.

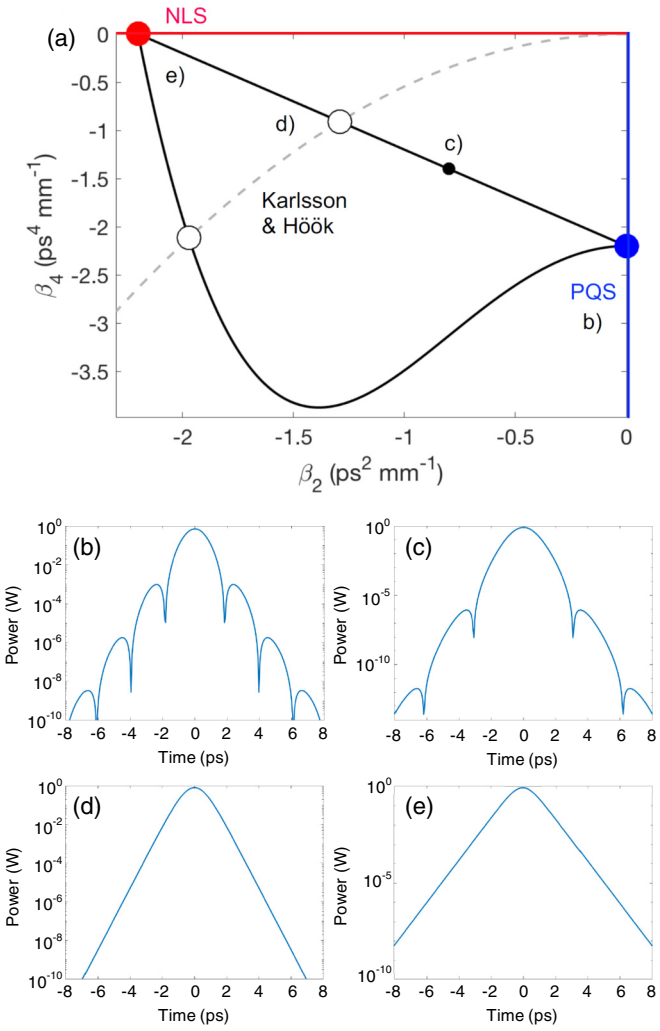

FIG. 1. (a) β_2 versus β_4 parameter space for fixed $\mu = 1.78$ mm^{-1}. The horizontal axis (red) represents conventional NLS solitons while the vertical axis (blue) represents PQSs. The grey dashed curve represents the family of Karlsson-Höök solutions at this value of μ. (b)–(e) Power (logarithmic scale) versus time for stationary solutions indicated in (a).

III. RELATIONSHIP BETWEEN PURE QUARTIC SOLITONS AND CONVENTIONAL SOLITONS

We search for stationary solutions to Eq. (4) which maintain their shapes throughout propagation, i.e.,

$$\psi(\tau, z) = u(\tau)e^{i\mu z}, \tag{7}$$

in the β_2, $\beta_4 < 0$ quadrant of parameter space in Fig. 1(a) bounded by PQSs (vertical axis, blue) and conventional solitons (horizontal axis, red). Here, and in the remainder of this paper, we only consider the case $\mu > 0$, which is associated with pulselike solutions; i.e., $\psi \to 0$ as $\tau \to \pm\infty$. Localized solutions do not exist for $\mu < 0$ due to resonance with the linear wave spectrum. With ansatz (7), Eq. (4) becomes a nonlinear ordinary differential equation for the temporal profile $u(\tau)$, which we take to be real to describe a uniform temporal phase, leading to

$$-\mu u - \frac{\beta_2}{2}u'' - \frac{|\beta_4|}{24}u'''' + \gamma u^3 = 0. \tag{8}$$

We solve Eq. (8) numerically by the Newton conjugate-gradient method [22]. Given a sufficiently accurate initial guess $u_0(\tau)$, the method converges upon the exact stationary solution $u(\tau)$ by computing successive corrections. We use known solutions such as the PQS or the NLS solitons as initial guesses $u_0(\tau)$ to a stationary solution at a nearby point in the β_2-β_4 parameter space [Fig. 1(a)]. By gradually modifying the dispersion parameters, we trace a path (black) in the parameter space and explore the limits of existence for soliton formation.

We define the two paths in the parameter space in Fig. 1(a) so as to link the PQS, indicated by the blue dot, with NLS solitons, indicated by the red dot. The paths are otherwise chosen arbitrarily, to illustrate that the PQS and the NLS solitons are connected to each other by small successive variations of the parameters β_2 and β_4. Indeed, we find that at each point along the path in Fig. 1(a), there is a soliton for any positive value of μ. To illustrate this, starting with the PQS, as indicated by the blue dot in Fig. 1(a), we show the power $|u|^2$ of the solution for a particular value of $\mu = 1.78$ mm^{-1} in Fig. 1(b). The oscillating tails are characteristic of PQSs [9]. As we approach the horizontal axis (red) corresponding to NLS solitons while keeping μ constant, the period of the oscillating tails increases [Fig. 1(c)], until the tails become exponentially decaying [Fig. 1(d)] as for NLS solitons [Fig. 1(e)]. Thus, we can continuously deform PQSs into NLS solitons, passing the analytic Karlsson and Höök solutions along the way [Fig. 1(d)]. Evidently there exists a general soliton family at each value of β_2, $\beta_4 < 0$ and peak power (specified by μ) which continuously joins all previously known classes of solutions: PQSs, conventional solitons, and the solutions reported by Karlsson and Höök [12].

The solutions we have found represent part of the GDKS superfamily. We now classify the members of this family and demonstrate that they are not limited to $\beta_2 < 0$.

IV. CLASSIFICATION OF THE GDKS SUPERFAMILY

We classify the GDKS family by an analytic description of their tails. In the low-power tails, we can discard the nonlinear term in Eq. (8) and find (see also [13,15,23,24])

$$-\mu u - \frac{\beta_2}{2}u'' - \frac{|\beta_4|}{24}u'''' = 0, \tag{9}$$

which has solutions that are linear combinations of terms of the form $e^{\lambda\tau}$, where the λ are given by

$$\lambda^2 = -\frac{6\beta_2}{|\beta_4|} \pm \sqrt{\frac{36\beta_2^2}{\beta_4^2} - \frac{24\mu}{|\beta_4|}}. \tag{10}$$

The roots λ are either all real ($\pm\lambda_1$, $\pm\lambda_2$) or occur in complex conjugate pairs ($\pm\lambda$, $\pm\lambda^*$). We classify these configurations on the β_2 versus μ parameter diagram of Fig. 2(a), with a fixed $\beta_4 = -1$ ps^4 mm^{-1}, which is a typical value for photonic crystal waveguides [8]. Let

$$\mu_0 \equiv \frac{3\beta_2^2}{2|\beta_4|} \tag{11}$$

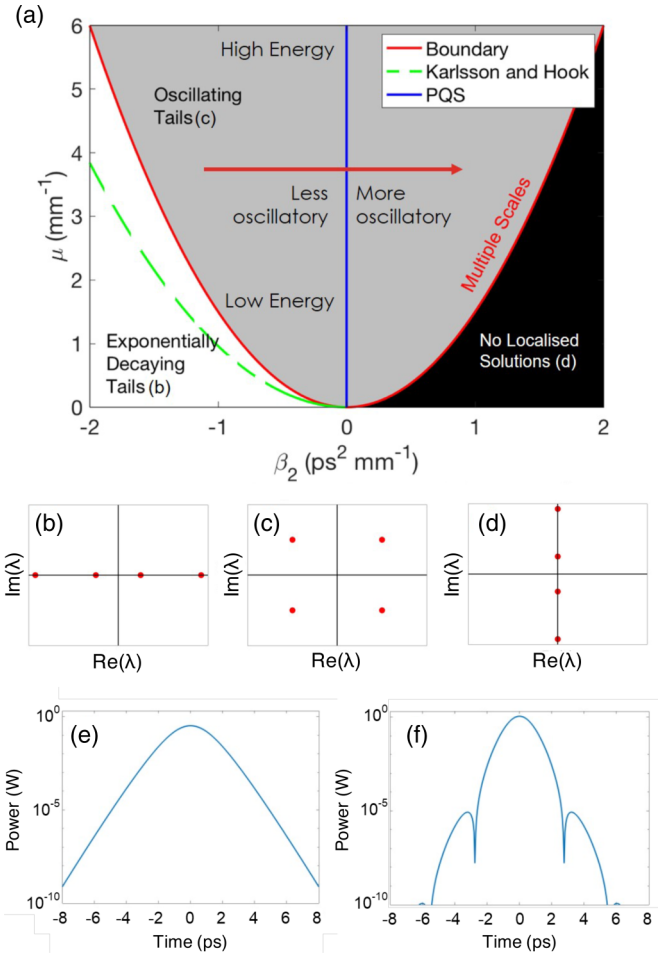

FIG. 2. (a) μ versus β_2 parameter diagram of solutions to Eq. (8), for fixed $\beta_4 = -1$ ps^4 mm^{-1}. (b)–(d) Configurations of roots λ in the complex plane [see Eq. (10)], corresponding to each of the colored regions in (a). (e) Power (logarithmic scale) versus time for the stationary solution corresponding to (b). (f) Same as in (e), but corresponding to (c).

denote the critical value of μ where the discriminant in Eq. (10) vanishes [13]. This results in a degeneracy where the roots λ become all real if $\beta_2 < 0$ and all imaginary if $\beta_2 > 0$. As such we have three regions in the parameter diagram of Fig. 2(a): $\mu > \mu_0$ (grey), $\mu < \mu_0$ and $\beta_2 < 0$ (white), and $\mu < \mu_0$ and $\beta_2 > 0$ (black). We discuss each of these regions in turn. We note that similar analyses has been carried out before. Akhmediev *et al.* [13] and Buryak and Akhmediev [15] considered the case of $\beta_2 < 0$, whereas Buffoni *et al.* [23] and Champneys and Toland [24] considered the case with quadratic nonlinearity.

A. $\beta_2 < 0$ and $\mu < \mu_0$

For $\beta_2 < 0$ and $\mu < \mu_0$, all λ's are real [Fig. 2(b)], so these solitons have exponentially decaying tails without oscillations [Fig. 2(e)]. These solutions are represented by the white region under the red parabola $\mu = \mu_0$ in Fig. 2(a). The solutions found by Karlsson and Höök [12], represented by Eq. (6), firmly lie within this region as expected from the sech^2 temporal profile [see Eq. (5)]. Since β_4 is fixed in Fig. 2(a), conventional solitons lie infinitely far to the left, which is also under the red parabola $\mu = \mu_0$.

B. $\beta_2 > 0$ and $\mu < \mu_0$

For $\beta_2 > 0$ and $\mu < \mu_0$, all λ's are imaginary [Fig. 2(d)]. As such, the linear tails are purely oscillatory. Therefore, in Fig. 2(a), there are no localized pulselike solutions in the black region under the red parabola $\mu = \mu_0$. As our focus is on localized solutions, we do not discuss this region further.

C. $\mu > \mu_0$

For $\mu > \mu_0$ and any β_2, λ is complex [Fig. 2(c)]. Although the nature of the linear exponentially decaying solutions we consider here does not guarantee the existence of pulselike nonlinear solutions [13], particularly for $\beta_2 > 0$, our numerical investigations outlined below indicate that such solutions indeed exist. These solutions are represented by the grey region above the red parabola $\mu = \mu_0$. The real part of λ gives the decay rate of the tails while the imaginary part gives the oscillation period. These solitons must have exponentially suppressed oscillations in the tails [Fig. 2(f)]. The exponential decay rate decreases when moving towards the right of the diagram, and so the solitons become increasingly wide. The PQSs, represented by the blue vertical axis, lie firmly within this region. For $\beta_2 < 0$, there is less than one oscillation per $e^{2\pi}$ increase in $u(\tau)$, whereas for $\beta_2 > 0$ there is more than one oscillation for the same increase. Figure 2(a) shows that for $\beta_2 > 0$ these solutions have a threshold in terms of μ. We comment on this in Sec. V.

V. META-ENVELOPE SOLITONS

We saw in Sec. IV C that solitons become increasingly wide on the right side of the parameter diagram in Fig. 2. Indeed, as we approach the red parabola in Fig. 2(a), i.e. $\mu \to \mu_0$, the characteristic time of decay in the tails becomes substantially larger than the period of oscillation, giving rise to solutions such as the blue curve in Fig. 3(a).

In this limit the solutions can be thought of as rapid oscillations, modulated by a slowly varying envelope [red curve in Fig. 3(a)]. Using multiple scales analysis [25], we isolate the envelope and neglect the oscillations which arise solely due to linear dispersion. To do this we introduce a small parameter ϵ, which is used to separate terms that differ greatly in magnitude.

We expand μ about the critical value μ_0 as defined in Eq. (11) by the parametrization

$$\mu = \mu_0(1 + \epsilon^2). \tag{12}$$

Equation (10) then becomes

$$\lambda^2 = -\frac{6\beta_2}{|\beta_4|}(1 \pm i\epsilon). \tag{13}$$

For $\epsilon \ll 1$, Eq. (13) reduces to

$$\lambda \approx \pm i\sqrt{\frac{6\beta_2}{|\beta_4|}}\left(1 \pm \frac{i\epsilon}{2}\right). \tag{14}$$

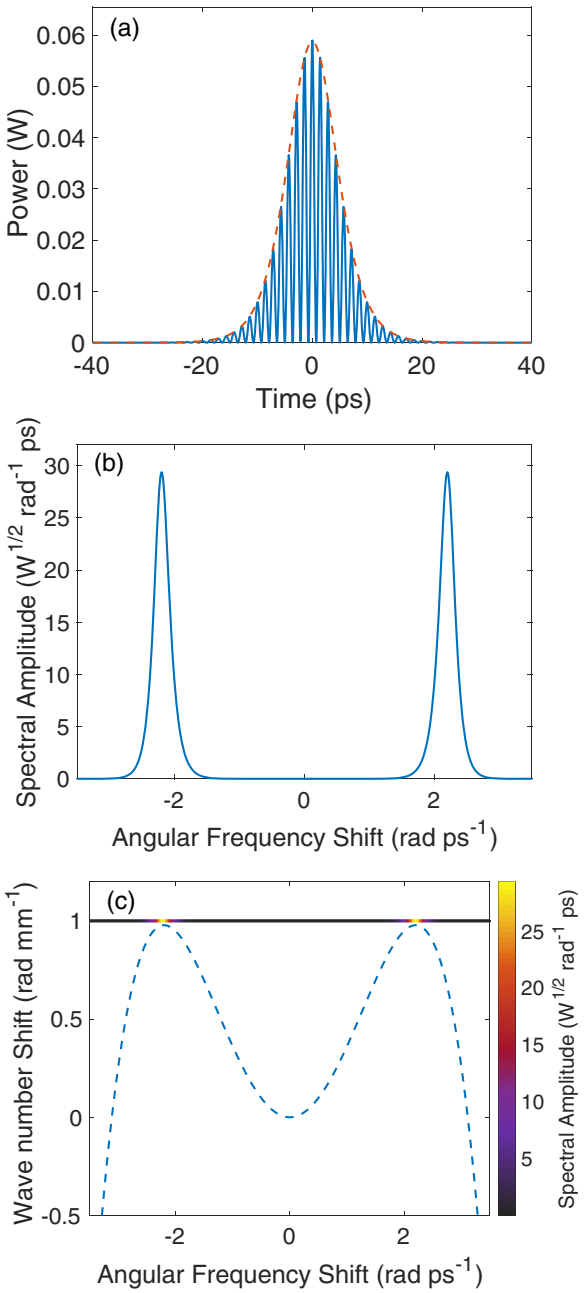

FIG. 3. (a) Power versus time for highly oscillatory solution (blue solid curve) for $\beta_4 = -1$ ps^4 mm^{-1}, $\beta_2 = 0.81$ ps^2 mm^{-1}, $\mu = 1$ mm^{-1}, and $\gamma = 1$ W^{-1} mm^{-1}. The corresponding meta-envelope is given by the red dashed curve. (b) Spectral amplitude of the stationary solution of (a). (c) Two-dimensional Fourier transform of the stationary solution of (a), with the spectral amplitude from (b) shown by the color scale. The linear dispersion relation is represented by the blue dashed curve.

The imaginary part gives an oscillation frequency

$$\omega_c \equiv \sqrt{6\beta_2/|\beta_4|}, \tag{15}$$

independent of ϵ. In the linear limit, $1/\pi\epsilon$ oscillations correspond to a $1/e$ decay in the tails. Thus, we are motivated to describe the soliton as

$$u(\tau) = \epsilon f(\epsilon\tau)\cos(\omega_c\tau), \tag{16}$$

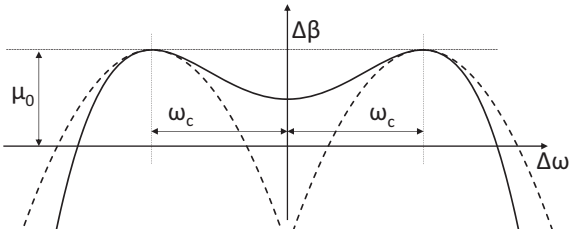

FIG. 4. Dispersion relation (17) (solid curve) for $\beta_2 > 0$ and $\beta_4 < 0$. When the frequency spectrum of the field is concentrated around the two maxima, the dispersion relation can be approximated by the dashed curve.

where, since ϵ is a small parameter, $\epsilon f(\epsilon\tau)$ is a slowly varying envelope. Recall, though, that $u(\tau)$ [blue curve in Fig. 3(a)] in Eq. (8) itself describes a wave envelope modulating an underlying carrier [5]. Thus $\epsilon f(\epsilon\tau)$ is in fact an envelope of an envelope, which we refer to as a meta-envelope [red dashed curve in Fig. 3(a)].

To understand the significance of the metacarrier frequency ω_c, consider the dispersion relation around ω_0, with $\beta_2 > 0$ and $\beta_4 < 0$:

$$\Delta\beta = \frac{\beta_2}{2}\Delta\omega^2 + \frac{\beta_4}{24}\Delta\omega^4, \tag{17}$$

where $\Delta\omega$ is the frequency offset from the expansion frequency ω_0, $\Delta\beta$ is the propagation constant offset from its value at ω_0, and β_2 and β_4 are the dispersion coefficients about $\Delta\omega = 0$. This dispersion relation is illustrated by the solid curve in Fig. 4. It has two maxima at $\Delta\omega = \pm\omega_c$, where $\Delta\beta$ takes the cutoff value μ_0 [see Eq. (11)]. As indicated in Fig. 3(c), the soliton dispersion relation for $\epsilon \ll 1$ (colored line) is thus on the verge of intersecting with the linear dispersion relation (blue dashed curve), which would lead to instability by radiation. The local curvature of the dispersion relation at $\pm\omega_c$ is negative (i.e., anomalous) and has the value $-2\beta_2$, as can be found by taking the second derivative of Eq. (17) at $\pm\omega_c$.

The meta-envelope f in ansatz (16) corresponds to the slowly varying envelope that multiplies the underlying carrier at the two maxima in the dispersion relation in Fig. 4. By the convolution theorem of Fourier transforms, we would expect the spectrum of $u(\tau)$ to be highly localized around those maxima, consistent with Figs. 3(b) and 3(c).

To continue our multiple scales analysis, we substitute Eqs. (12) and (16) into Eq. (8), and equate terms of the same order in ϵ. The $O(\epsilon)$ and $O(\epsilon^2)$ terms are found to be

$$O(\epsilon):\ -\mu_0 f\cos(\omega_c\tau) + \omega_c^2\frac{\beta_2}{2}f\cos(\omega_c\tau) - \omega_c^4\frac{|\beta_4|}{24}f\cos(\omega_c\tau) = 0,$$
$$O(\epsilon^2):\ \omega_c\beta_2 f'\sin(\omega_c\tau) - \omega_c^3\frac{|\beta_4|}{6}f'\sin(\omega_c\tau) = 0. \tag{18}$$

The first of these is satisfied because we have chosen ω_c to satisfy Eq. (17) when $\Delta\beta = \mu_0$. The second is satisfied because at $\pm\omega_c$ the inverse group velocity vanishes. The first

nontrivial result then comes at $O(\epsilon^3)$, for which

$$-\mu_0 f\cos(\omega_c\tau) - \frac{\beta_2}{2}f''\cos(\omega_c\tau) + \omega_c^2\frac{|\beta_4|}{4}f''\cos(\omega_c\tau) + \gamma f^3\cos^3(\omega_c\tau) = 0. \quad (19)$$

We truncate the perturbation expansion at $O(\epsilon^3)$. This means that we neglect cubic and quartic dispersion in the two narrow frequency ranges for which the meta-envelope spectrum is appreciable [see Figs. 3(b) and 3(c)] and corresponds to approximating dispersion relation (17) by the dashed curve in Fig. 4, which has the same value and curvature as the original dispersion relation at $\Delta\omega = \pm\omega_c$.

We now rewrite Eq. (19) as

$$-\mu_0 f\cos(\omega_c\tau) - \frac{-2\beta_2}{2}f''\cos(\omega_c\tau) + \gamma f^3\cos^3(\omega_c\tau) = 0.$$

Multiplying by $\cos(\omega_c\tau)$ and averaging over a period gives an NLS equation for the meta-envelope:

$$-\mu_0 f - \frac{-2\beta_2}{2}f'' + \frac{3}{4}\gamma f^3 = 0. \quad (20)$$

We recover the full spatial dependence if we take the ansatz $\psi(\tau, z) = \epsilon f(\epsilon\tau)\cos(\omega_c\tau)\,\exp(i\mu_0(1+\epsilon^2)z)$ in Eq. (4).

$$i\frac{\partial F}{\partial Z} - \frac{-2\beta_2}{2}\frac{\partial^2 F}{\partial T^2} + \frac{3}{4}\gamma F^3 = 0, \quad (21)$$

where $Z = \epsilon^2 z$, $T = \epsilon\tau$, and $F = \epsilon f(T)\exp(i\mu_0 Z)$ are slowly varying variables. Equation (21) may be recognized as the nonlinear Schrödinger equation. Although the quadratic dispersion is normal at the expansion frequency ω_0, the effective quadratic dispersion parameter in Eq. (21) is $\beta_{2,c} = -2\beta_2$, corresponding to the anomalous dispersion at the actual carrier frequency $\Delta\omega = \pm\omega_c$. The effective nonlinearity is reduced to $3\gamma/4$ since a fraction $\gamma/4$ is associated with the third harmonic, i.e.,

$$\cos^3(\omega_c\tau) = \tfrac{3}{4}\cos(\omega_c\tau) + \tfrac{1}{4}\cos(3\omega_c\tau). \quad (22)$$

The fact that the nonlinear Schrödinger equation arises in this context is perhaps not surprising since it generally can be shown to apply to the envelope of nonlinear Hamiltonian systems [25].

Equation (21) is solved by hyperbolic secant-shaped meta-envelopes

$$F(T, Z) = 2\epsilon\sqrt{\frac{\beta_2^2}{\gamma|\beta_4|}}\,\mathrm{sech}\left(\sqrt{\frac{3\beta_2}{2|\beta_4|}}T\right)e^{i\mu_0 Z}. \quad (23)$$

We refer to these as fundamental metasolitons, in analogy to the conventional fundamental solitons. We have tested the accuracy of this meta-envelope description by comparing with numerical solutions of the full Eq. (8). Figure 5 shows that the percentage error in peak power predicted by Eq. (23) is less than 10% for $\epsilon < 0.6$.

Higher-order metasolitons, in analogy to higher-order conventional solitons, would also be expected [26]. In Fig. 6(a), we multiply the amplitude of a highly oscillatory solution ($\epsilon = 0.05$) by a factor of $N = 2$, where N is analogous to the soliton number for conventional solitons. By the split-step numerical method, we simulate its propagation. As shown in Fig. 6(b), the meta-envelope periodically contracts and returns to its original shape, similar to higher-order conventional solitons. The period of evolution is as expected from soliton theory,

$$L_m = \frac{\pi}{2}L_{GVD} = \frac{\pi T_0^2}{4|\beta_2|}, \quad (24)$$

where

$$T_0 = \sqrt{\frac{2|\beta_4|}{3\beta_2}}\frac{1}{\epsilon} \quad (25)$$

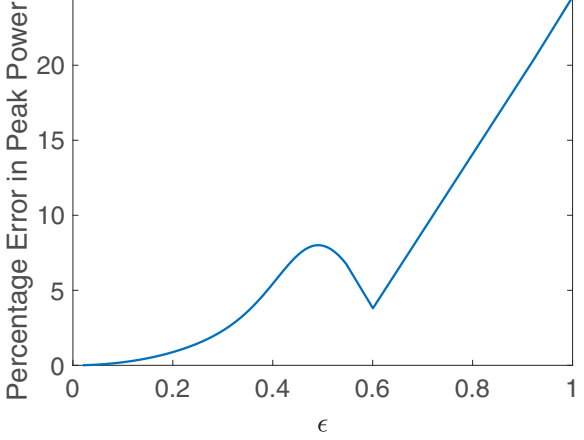

FIG. 5. Percentage error in the meta-envelope peak power compared with numerical solutions as a function of the expansion parameter ϵ.

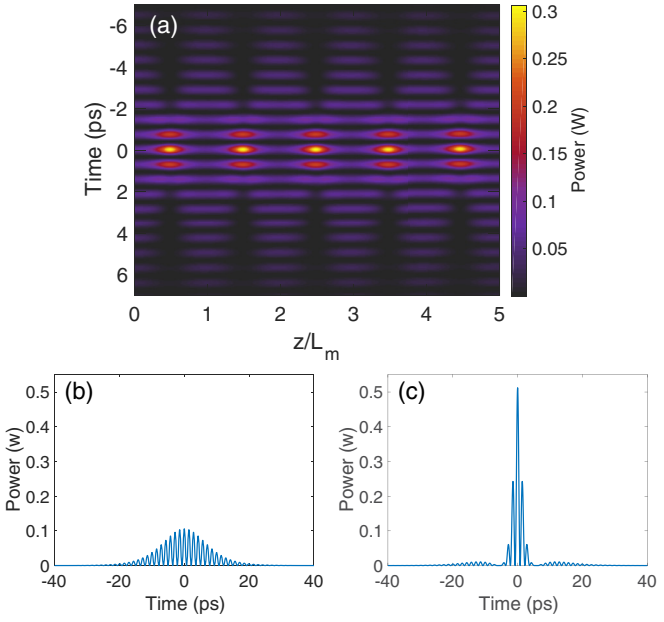

FIG. 6. (a) Power versus time at various propagation distances for stationary solution of Fig. 3 multiplied with an amplitude multiplier $N = 2$. (b) Power versus time for the input pulse in (a). (c) Pulse in (b) after propagation by five metasoliton periods $\pi T_0^2/(4|\beta_2|)$.

is the half width at $\mathrm{sech}^2(1) \approx 0.42$ of the intensity maximum of the meta-envelope. Over this metasoliton period, the radiation of energy into dispersive waves is gradual, which indicates that deviations from the meta-envelope description are small.

Having found the metasoliton solutions, we can now understand the finite threshold of μ for $\beta_2 > 0$. As discussed below Eq. (17), at the expansion frequency ω_0 the dispersion is normal and bright solitons thus do not exist at low peak powers. Solitons are only possible once the peak power reaches a threshold, where the soliton spectrum attains sufficient width so as to sense the anomalous dispersion at $\Delta\omega = \pm\omega_c$.

VI. SCALING OF GDKS

The generalized NLS equation (8) is invariant under the following rescaling of the amplitude u, temporal and spatial coordinates τ and z, and dispersion coefficients β_2 and β_4:

$$u \to \alpha u, \quad \mu \to \alpha^2 \mu,$$
$$\beta_2 \to \delta^{1/2}\alpha\beta_2, \quad \beta_4 \to \delta\beta_4, \quad \tau \to \delta^{1/4}\alpha^{-1/2}\tau. \quad (26)$$

To see the significance of such a transformation, consider first the case where $\delta = 1$. This keeps β_4 constant and thus generates the entire parameter diagram of Fig. 2. The values of β_2 and μ that result as α varies lie on the same half parabola $\mu \sim \beta_2^2$ as the original values. Thus, all the stationary solutions on such half parabolas, such as the Karlsson-Höök solutions given by Eq. (6), are simply rescaled versions of one another with altered peak powers and pulse widths. Likewise, for equal values of ϵ [see Eq. (12)], the metasoliton solutions discussed in Sec. V are related by this transformation. Seen this way, the PQS corresponds to the degenerate case where the two half parabolas coincide.

In the general case of the transformations of Eq. (26), the combination $\mu|\beta_4|/\beta_2^2$ remains unchanged. We thus define the dimensionless GDKS shape parameter as

$$\sigma = \sqrt{\frac{3}{2\mu|\beta_4|}}\beta_2, \quad (27)$$

where the factor 3/2 was included such that $\sigma = \pm 1$ corresponds to the red parabola separating the various regions in Fig. 2. $\sigma = 0$ corresponds to the PQSs (blue line in Fig. 2). The Karlsson-Höök solutions [green dashed curve in Fig. 2; Eq. (6)] are given by $\sigma = -5/4$. No localized solutions exist for $\sigma > 1$.

We can reformulate the generalized NLS equation (8) in terms of the GDKS parameter. Suppose we parametrize $\beta_2 = \sigma\sqrt{2\mu|\beta_4|/3}$ in terms of σ. Equation (8) then becomes

$$-u - \sigma\sqrt{\frac{|\beta_4|}{6\mu}}u'' - \frac{|\beta_4|}{24\mu}u'''' + \gamma u^3 = 0. \quad (28)$$

If we define a normalized amplitude and time as

$$U = \sqrt{\frac{\gamma}{\mu}}u, \quad T = \left(\frac{24\mu}{|\beta_4|}\right)^{1/4}\tau, \quad (29)$$

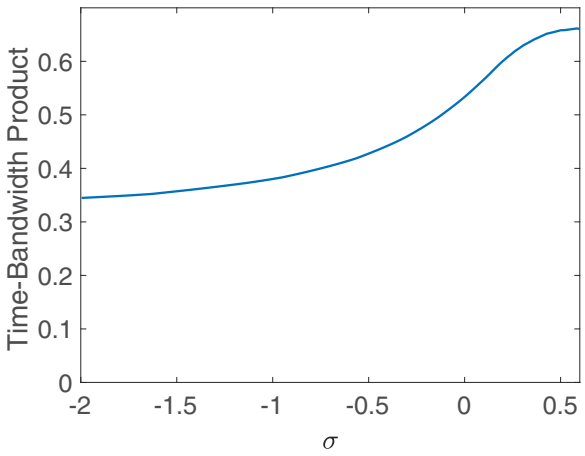

FIG. 7. Time-bandwidth product versus GDKS shape parameter σ.

then Eq. (28) becomes

$$U + 2\sigma U'' + U'''' = U^3. \quad (30)$$

Thus this system of mixed quadratic and quartic dispersion is solely characterized by the GDKS shape parameter, which describes the relative strength of β_2 and β_4. As we increase the peak power and thus μ, larger values of β_2 are required to maintain the same value of σ. This is because the solutions become spectrally wider and the quartic dispersion thus becomes more dominant over quadratic dispersion for a fixed value of β_4.

Each value of $\sigma < 1$ describes a family of solitons existing for all values of β_2 and β_4 with the appropriate signs, and that are related by the scaling relations (26). In other words, all the solutions which exist in the three-dimensional parameter space (β_2, β_4, μ) can be represented by a single parameter σ. Solutions with the same value of σ have the same shape; i.e., they are related to each other by linear transformations of the horizontal and vertical axes. A similar one-parameter parametrization was reported earlier by Akhmediev *et al.* [13]. The solutions at each σ can thus be characterized by quantities that are invariant under the transformations (26). One such quantity is the time-bandwidth product, which is the product of the full width at half maximum of the temporal and spectral intensity profiles. The time-bandwidth product (TBP) versus σ is shown in Fig. 7. It is not well defined in the meta-envelope region ($\sigma \to 1$), where the temporal profile becomes increasingly oscillatory [see Fig. 3(a)], since the spectrum develops two distinct maxima. This is why we only show results for $\sigma < 0.5$. Note that the time-bandwidth product increases monotonically with σ. At $\sigma = 0$ we find that the time-bandwidth product is 0.53, consistent with the result found earlier for PQSs [9]. As σ becomes large and negative it approaches the value 0.32 for hyperbolic secant pulses. This means that, for the same pulse duration, the pulse's bandwidth increases with increasing σ. This is not surprising, perhaps, since the oscillations in the tails, the amplitude of which increases with σ, introduce additional frequencies that lead to spectral broadening. We note that another natural choice of metric, the root-mean-square time-bandwidth product, diverges for $\sigma > 0.5$.

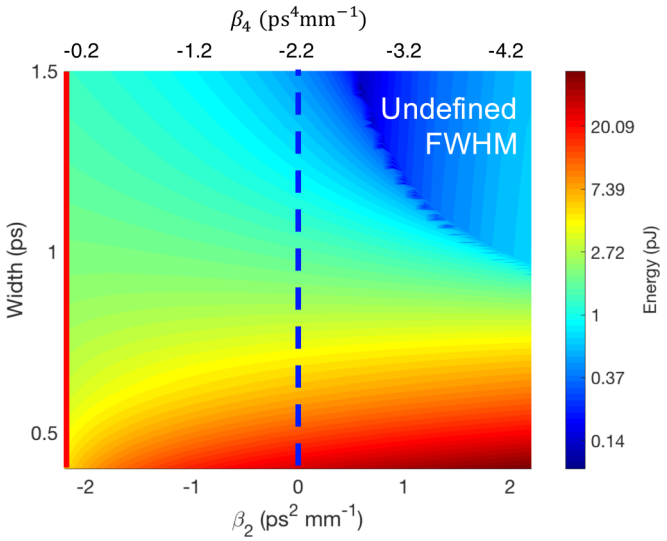

FIG. 8. Energy of stationary solutions versus specified values of β_2 and β_4 (varying according to the straight part of the contour in Fig. 1) and pulse width. Red solid line represents the NLS solitons while the blue dashed line represents the PQSs.

We now turn to the energy-width scaling within the GDKS family. To contrast the effects of varying β_2 and β_4, we focus on solutions which lie on the black line in the β_2-β_4 parameter plane of Fig. 1(a), which joins a conventional soliton (red) with a PQS (blue). The corresponding values of β_2 and β_4 are shown on the horizontal axis of Fig. 8, which shows the pulse energy (color scale) as a function of pulse width w (vertical axis) for the specified values of the dispersion parameters. To provide some idea of the magnitudes of these parameters, we have chosen the dispersion parameters to be consistent with those in the experiments of Blanco-Redondo *et al.* [8].

The figure shows that for long pulses, the highest pulse energies lie to the left in Fig. 8. This means that negative β_2 is more important than negative β_4 in achieving high pulse energies at relatively large pulse widths. The top right of the diagram corresponds to the highly delocalized solutions when $\beta_2 > 0$, for which the full width at half maximum is not well defined. In contrast, for sufficiently narrow pulses, the highest pulse energies lie to the right of Fig. 8, beyond even the PQSs (blue dashed line). This implies that in the design of soliton supporting platforms, it is possible to go beyond the advantageous PQS energy scaling [2, Runge *et al.*] by considering a dispersion relation with moderate positive values of β_2. However, this comes at the expense of more oscillatory behavior in the tails of the pulses. This presents a clear trade-off in laser applications, for instance, where a higher energy at a fixed width can be obtained at the expense of increasingly prominent oscillations in the tails.

VII. EFFECTS OF CUBIC DISPERSION: $\beta_3 \neq 0$

Having ignored cubic dispersion until now, we turn to its effect on GDKS formation. The generalized NLS equation that includes β_3 reads

$$i\frac{\partial\psi}{\partial z} - \frac{\beta_2}{2}\frac{\partial^2\psi}{\partial\tau^2} - \frac{i\beta_3}{6}\frac{\partial^3\psi}{\partial\tau^3} - \frac{|\beta_4|}{24}\frac{\partial^4\psi}{\partial\tau^4} + \gamma|\psi|^2\psi = 0, \quad (31)$$

This equation was studied by Piché *et al.* [16], who showed that when β_3 is sufficiently small, corresponding to $\beta_2(\omega)$ not changing sign over the width of the pulse spectrum, then the pulse moves slowly with respect to the rest frame but is otherwise unchanged. Stationary solutions for nonzero β_3, for which the phase depends on τ, were reported by Kruglov and Harvey [27]. However, such a time dependence can be interpreted as a shift $\Delta\omega$ in the carrier frequency away from the expansion frequency ω_0 where the dispersion parameters $\beta_{2,3,4}$ were defined by Taylor expansion. Indeed it is more natural to perform this expansion about the actual carrier frequency $\omega_0 + \Delta\omega$. The value of $\Delta\omega$ in the solutions of Kruglov and Harvey corresponds to the unique frequency on a quartic dispersion relation where β_3 vanishes:

$$\Delta\omega = -\frac{\beta_3}{\beta_4}. \quad (32)$$

As such, the solutions of Kruglov and Harvey, which also have a sech^2 amplitude profile, are the Karlsson-Höök solutions [Eq. (5)] when viewed in the more natural rest frame of the carrier, where $\beta_3 = 0$.

Now consider a more general ansatz for a moving solitary wave:

$$\psi(\tau, z) = u\left(\tau - \frac{z}{v}\right)e^{i\mu z}, \quad (33)$$

where the real amplitude profile u now travels at an inverse velocity v^{-1} relative to the rest frame of the expansion frequency ω_0. Substituting Eq. (33) into Eq. (31), the imaginary part gives

$$-\frac{1}{v}u' - \frac{\beta_3}{6}u''' = 0 \quad (34)$$

as an additional constraint to the (real) Eq. (8). We have found that this additional constraint is inconsistent with the solutions to Eq. (8), unless $v^{-1} = 0$, which means that the group velocity of the pulse is equal to that at $\omega = \omega_0$. We thus find that for real u, the generalized ansatz (33) does not contribute solutions in addition to the solutions following from ansatz (7).

VIII. DYNAMICS

We now turn to the dynamical properties of GDKSs. We apply small normal mode perturbations $f, g \ll 1$ to a GDKS $u(\tau)$ [28]:

$$\psi(\tau, z) = (u(\tau, z) + f(\tau)e^{\Lambda z} + g^*(\tau)e^{\Lambda^* z})e^{i\mu z}. \quad (35)$$

Λ and Λ^* are eigenvalues characterizing the evolution of the conjugate modes f and g, which are coupled by the nonlinearity. Substituting Eq. (35) into Eq. (4) and retaining only terms linear in f and g gives the system of coupled ordinary differential equations

$$\begin{aligned} -\frac{\beta_2}{2}f'' - \frac{|\beta_4|}{24}f'''' + (2\gamma u^2 - \mu)f + \gamma u^2 g &= -i\Lambda f, \\ \frac{\beta_2}{2}g'' + \frac{|\beta_4|}{24}g'''' - (2\gamma u^2 - \mu)g - \gamma u^2 f &= -i\Lambda g. \end{aligned} \quad (36)$$

These may be solved numerically by expressing f and g in terms of Fourier series [22]. The linearized eigenspectrum of

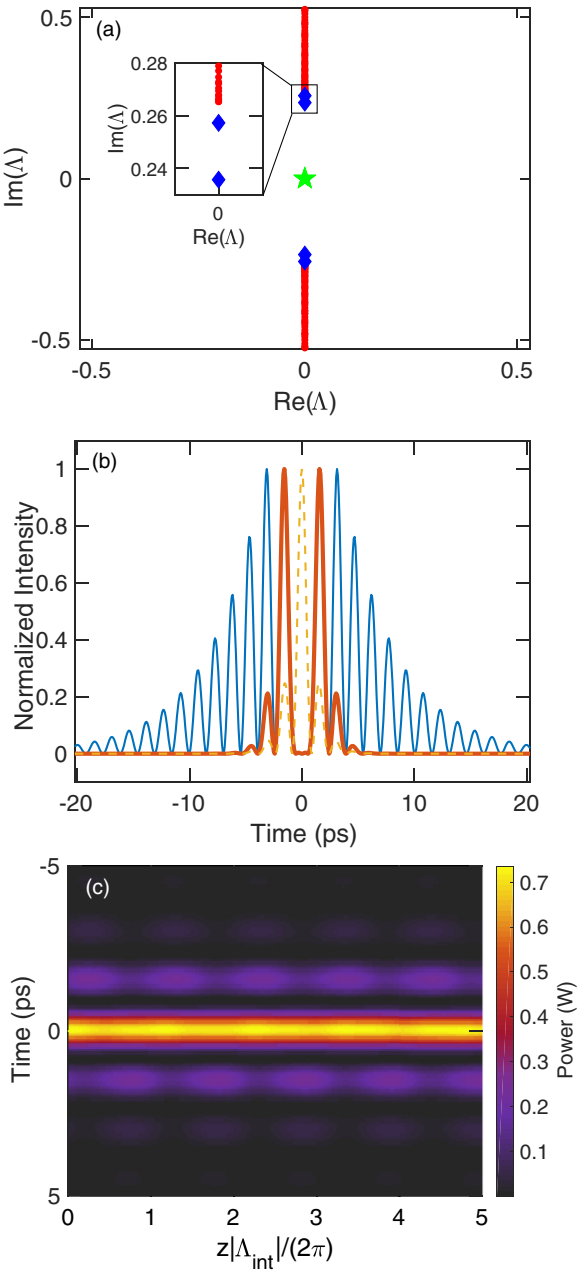

FIG. 9. (a) Linearized eigenspectrum for the GDKS with $\beta_2 = 0.7$ ps^2 mm^{-1}, $\beta_4 = 1$ ps^4 mm^{-1}, and $\mu = 1$ mm^{-1}. Red points represent high-spatial-frequency perturbations which are radiated as dispersive waves. The green star represents the zero eigenvalues corresponding to the translational and phase invariance of Eq. (4). Blue diamonds represent discrete internal modes. (b) Conjugate mode profiles f (thick red solid curve) and g (thin blue solid curve) corresponding to the larger internal mode eigenvalue of (a), with the soliton shown for comparison (yellow dashed curve). (c) Power versus time for the GDKS in (a) perturbed by the internal mode in (b) over five internal mode oscillation periods $T_{\rm int}$.

the GDKS for $\beta_2 = 0.7$ ps^2 mm^{-1}, $\beta_4 = -1$ ps^4 mm^{-1}, and $\mu = 1$ mm^{-1} is shown in the complex plane in Fig. 9(a). We observe that all eigenvalues Λ are imaginary, indicating that no linear perturbations grow exponentially. We have observed that the entire GDKS family is linearly stable.

We focus on the features of the eigenspectrum in Fig. 9(a). The green star shows the zero eigenvalues which correspond to the translational and phase invariance of Eq. (4). The red lines represent a continuum of high-spatial-frequency modes which are unbound by the potential of the soliton. Such perturbations radiate into the far field as dispersive waves. Isolated discrete eigenvalues (blue diamonds), which must occur in conjugate pairs, correspond to internal modes [28]. These are persistent small-amplitude shape oscillations which decay only by the nonlinear generation of higher harmonics lying within the dispersive wave continuum. Unlike NLS solitons, which have no internal modes [29], and the single symmetric internal mode of the PQS [9], the GDKS in Fig. 9(a) has two internal modes. The smaller eigenvalue corresponds to a symmetric mode, where energy is exchanged between the central maximum and the adjacent tail maxima. In contrast, the larger eigenvalue represents an antisymmetric mode where energy is exchanged between the two sides of the pulse while the central maximum remains unchanged. This mode profile is shown in Fig. 9(b). The thick red and thin blue solid curves depict the conjugate modes f and g corresponding to the shapes of different phases of the shape oscillation. The yellow dashed curve shows the soliton for comparison.

Figure 9(c) shows the result of subjecting the GDKS to a 5% perturbation by the antisymmetric internal mode of Fig. 9(b). The observed oscillation period is as predicted by

$$T_{\rm int} = \frac{2\pi}{|\Lambda_{\rm int}|}, \tag{37}$$

where $\Lambda_{\rm int}$ is the internal mode eigenvalue. We can also observe such internal modes by generating GDKSs from Gaussian inputs in split-step propagation simulations. As the pulse sheds energy in order to develop the correct shape of a GDKS, the internal mode(s) of the corresponding soliton is excited, leading to out-of-phase oscillations in the peak power and temporal width of the pulse. The equilibrium peak power and pulse width of such oscillations match the values for our numerical solutions to the GDKS superfamily.

While a complete characterization of the internal modes throughout the parameter plane of Fig. 2 is beyond our current scope, the single internal mode observed for the PQS [9] appears to vanish for sufficiently large values of $|\beta_2|$. In this case, we expect all oscillations in peak power and pulse width upon perturbation to be exponentially damped. As we approach the metasoliton regime, multiple internal mode eigenvalues bifurcate from the continuum and beat with one another upon excitation. Sufficiently close to the cutoff $\mu = \mu_0$ we expect to observe no internal modes due to the integrability of the meta-envelope NLS equation (21).

IX. DISCUSSION AND CONCLUSIONS

We have provided a comprehensive description of solitons in the presence of a Kerr nonlinearity and quadratic and quartic dispersion. We propose the term generalized dispersion Kerr solitons to refer to the superfamily of soliton solutions existing in this parameter space, which includes the notable cases of NLS solitons and PQSs, and which are characterized by the single parameter σ. Since dispersion relations domi-

nated by an even order of dispersion can at least in principle be isolated from the soliton spectrum, we might infer that this superfamily should also encompass soliton solutions in the presence of higher orders of even dispersion (β_6, β_8, etc.), although a systematic study of these solutions remains to be carried out.

We note that for the solutions we have discussed, their frequency and wave number content do not overlap with the linear dispersion relation. This is illustrated, for example, in Fig. 3(c), which shows a small but finite gap between the dashed curve, which represents the linear dispersion relation, and the horizontal line, which represents the nonlinear pulse. By the argument of Akhmediev and Karlsson [30], this implies that the nonlinear pulse is stable against radiation losses, consistent with the analysis in Sec. VIII.

One of our satisfying findings is that the solutions found by Karlsson and Höök [12] naturally fit in the classification outlined in Fig. 2. One reason, perhaps, why analytic solutions can be found is that, for the associated μ given in Eq. (6), the exponential tails are superpositions of terms that vary as $e^{\pm\lambda\tau}$ and $e^{\pm 2\lambda\tau}$. In other words, deep in the tails the exponential decay rates differ by exactly a factor of 2. It is straightforward to see that in the presence of a Kerr nonlinearity this leads to terms of the form $e^{\pm m\lambda\tau}$, where m is a positive integer. This may motivate the search for analytic solutions where the decay rates are related by other simple rational ratios.

In Sec. VII we discussed aspects of the effect of β_3. As a more general comment than the particular discussion in that section, we note that we did not find any solutions when $\beta_3 \neq 0$, consistent with ansatz (7). This means that all solutions we find travel at the group velocity $1/\beta_1$ at the frequency where $\beta_3 = 0$. For the conventional nonlinear Schrödinger equation, which exhibits Galilean invariance, solutions exist for all frequencies for which $\beta_2 < 0$, each with an associated group velocity. However, the inclusion of quartic dispersion removes the Galilean invariance, and so this property does not carry over. Another way to see this is that changing the frequency, and neglecting dispersion orders higher than four, changes $\beta_{1,2,3}$, leading to a different equation. Of course, the fact that we do not find solutions for nonzero β_3 does not mean that such solutions do not exist; it merely means that a more complicated ansatz than Eq. (7), or its direct generalizations [27], is required.

We have found that, for highly oscillatory metasoliton solutions, their basin of attraction does not seem to include Gaussian-like inputs. In such cases, we have numerically demonstrated that it is possible to generate such solitons by adiabatically varying the dispersion profile of the system. Further work is required to find the threshold value of β_2 where a GDKS can be generated for a given Gaussian input pulse.

Our discussion in Sec. VI, and in particular the information in Figs. 7 and 8, shows that for applications in soliton lasers finding the optimal ratio of β_2 and β_4 is subtle. Figure 8 shows that a combination of negative quartic dispersion and some positive quadratic dispersion can lead to high pulse energies. On the other hand, if the quadratic dispersion becomes too large then the oscillations become prominent and the time-bandwidth product increases. Irrespective of these subtleties though, our results show that pure quadratic dispersion is unlikely to be optimal, and that investigating and leveraging different orders of dispersion can be expected to be worthwhile to maximize laser performance.

In summary, we have provided a unifying framework to understand nonlinear pulse propagation in systems with different significant dispersion orders. From an applications standpoint our findings may have practical implications in ultrafast laser design where new energy scaling laws and pulse shapes become available.

ACKNOWLEDGMENTS

This work was supported by the Australian Research Council (Grant No. DP180102234). A.B.-R. acknowledges a University of Sydney Professor Harry Messel Fellowship.

[1] C. S. Gardner, J. M. Greene, M. D. Kruskal, and R. M. Miura, Phys. Rev. Lett. **19**, 1095 (1967).
[2] L. Khaykovich, F. Schreck, G. Ferrari, T. Bourdel, J. Cubizolles, L. D. Carr, Y. Castin, and C. Salomon, Science **296**, 1290 (2002).
[3] V. M. Pérez-García, H. Michinel, and H. Herrero, Phys. Rev. A **57**, 3837 (1998).
[4] N. J. Zabusky and M. D. Kruskal, Phys. Rev. Lett. **15**, 240 (1965).
[5] G. P. Agrawal, *Nonlinear Fiber Optics*, 5th ed. (Elsevier, Amsterdam, 2012), Chap. 5.
[6] K. I. Pushkarov, D. I. Pushkarov, and I. V. Tomov, Opt. Quantum Electron. **11**, 471 (1979).
[7] P. G. Kevrekidis and D. J. Frantzeskakis, Rev. Phys. **1**, 140 (2016).
[8] A. Blanco-Redondo, C. M. de Sterke, J. E. Sipe, T. F. Krauss, B. J. Eggleton, and C. Husko, Nat. Commun. **7**, 10427 (2016).
[9] K. K. K. Tam, T. J. Alexander, A. Blanco-Redondo, and C. M. de Sterke, Opt. Lett. **44**, 3306 (2019).
[10] C. W. Lo, A. Stefani, C. M. de Sterke, and A. Blanco-Redondo, Opt. Express **26**, 7786 (2018).
[11] H. Taheri and A. B. Matsko, Opt. Lett. **44**, 3086 (2019).
[12] M. Karlsson and A. Höök, Opt. Commun. **104**, 303 (1994).
[13] N. Akhmediev, A. Buryak, and M. Karlsson, Opt. Commun. **110**, 540 (1994).
[14] N. N. Akhmediev and A. V. Buryak, Opt. Commun. **121**, 109 (1995).
[15] A. V. Buryak and N. N. Akhmediev, Phys. Rev. E **51**, 3572 (1995).
[16] M. Piché, J.-F. Cormier, and X. Zhu, Opt. Lett. **21**, 845 (1996).
[17] S. Roy and F. Biancalana, Phys. Rev. A **87**, 025801 (2013).
[18] A. Bansal, A. Biswas, Q. Zhou, and M. M. Babatin, Optik **169**, 12 (2018).

[19] A. Biswas, H. Triki, Q. Zhou, S. P. Moshokoa, M. Z. Ullah, and M. Belic, Optik **144**, 357 (2017).
[20] I. P. Christov, M. M. Murnane, H. C. Kapteyn, J. Zhou, and C.-P. Huang, Opt. Lett. **19**, 1465 (1994).
[21] G. P. Agrawal, *Nonlinear Science at the Dawn of the 21st Century* (Springer, Berlin, 2000), pp. 195–211.
[22] J. Yang, *Nonlinear Waves in Integrable and Nonintegrable Systems* (SIAM, Philadelphia, 2010), Vol. 16.
[23] B. Buffoni, A. R. Champneys, and J. F. Toland, J. Dyn. Differ. Equations **8**, 221 (1996).
[24] A. R. Champneys and J. F. Toland, Nonlinearity **6**, 665 (1993).
[25] R. K. Dodd, J. C. Eilbeck, J. D. Gibbon, and H. C. Morris, *Solitons and Nonlinear Wave Equations* (Academic Press, New York, 1982), Chap. 8.
[26] J. Satsuma and N. Yajima, Prog. Theor. Phys. Suppl. **55**, 284 (1974).
[27] V. I. Kruglov and J. D. Harvey, Phys. Rev. A **98**, 063811 (2018).
[28] Y. S. Kivshar, D. E. Pelinovsky, T. Cretegny, and M. Peyrard, Phys. Rev. Lett. **80**, 5032 (1998).
[29] D. E. Pelinovsky, Y. S. Kivshar, and V. V. Afanasjev, Physica D **116**, 121 (1998).
[30] N. Akhmediev and M. Karlsson, Phys. Rev. A **51**, 2602 (1995).